

Design of a Frequency Domain Instrument for Simultaneous Optical Tomography and Magnetic Resonance Imaging of Small Animals

James M. Masciotti^{*a}, Shaheed Rahim^b, Jarrett Grover^a, Andreas H. Hielscher^{*a,b}

^aDept. of Biomedical Engineering, Columbia Univ., 500 West 120th St., New York, NY USA 10027

^bDept. of Radiology, Columbia Univ., 660 West 168th St., New York, NY USA 10032

ABSTRACT

We present a design for frequency domain instrument that allows for simultaneous gathering of magnetic resonance and diffuse optical tomographic imaging data. This small animal imaging system combines the high anatomical resolution of magnetic resonance imaging (MRI) with the high temporal resolution and physiological information provided by diffuse optical tomography (DOT). The DOT hardware comprises laser diodes and an intensified CCD camera, which are modulated up to 1 GHz by radio frequency (RF) signal generators. An optical imaging head is designed to fit inside the 4 cm inner diameter of a 9.4 T MRI system. Graded index fibers are used to transfer light between the optical hardware and the imaging head within the RF coil. Fiducial markers are integrated into the imaging head to allow the determination of the positions of the source and detector fibers on the MR images and to permit co-registration of MR and optical tomographic images. Detector fibers are arranged compactly and focused through a camera lens onto the photocathode of the intensified CCD camera.

Keywords: Frequency Domain, Optical Tomography, Small Animal Imaging, Multimodality

1. INTRODUCTION

Small animals, such as mice and rats, are increasingly used by researchers as models for human diseases. The imaging of these animals allows researchers to explore anatomical and physiological changes *in vivo* during disease progression and over the course of various treatment regimens [1-5]. There are many different biomedical imaging modalities that can be used, each having their own advantages and disadvantages. Although one imaging modality maybe better suited than another for a given application, seldom does a single imaging modality provide one with all desired information. Therefore increasing attention has been focused on combining two or more biomedical imaging modalities. Two such imaging modalities which have complimentary characteristics are magnetic resonance imaging (MRI) and diffuse optical tomography (DOT).

MRI is a well-established imaging modality that is capable of yielding anatomical images of soft tissue with high spatial resolution [6]. With MRI, nuclei, usually ¹H, are excited by radio frequency (RF) electromagnetic pulses. After nuclei have been excited they relax and release the energy in the form of RF and this signal is measured by the detection hardware. A high magnetic field is required for a sufficient MRI signal. Human MRI scanners typically have field strengths ranging from 0.3T to 3T. For the high spatial resolution required by small animal imaging, higher field strengths ranging from 7T to 11.7T are used. Having large field strength usually limits the bore size in which a target can be imaged. The imaging space where a small animal can be placed is a cylinder with a diameter ranging from 2 to 5 cm. Smaller diameters usually yield better signal to noise (SNR) ratios. Conventionally, tissue contrast is produced in part by spin densities and certain nuclear magnetic properties such as relaxation time constants T1 and T2. Slice thicknesses can be as small as 200 μ m while the in-plane resolution can be as small as 50 μ m. Images can also be parametrically generated to show blood volume and blood flow. Furthermore, a variant of MRI called functional magnetic resonance imaging, fMRI, allows the imaging of properties that vary in time. This technique has temporal resolution on the order of 0.5 Hz, and has significantly less SNR than conventional MRI.

Diffuse Optical Tomography is an emerging imaging modality [7]. It uses non-ionizing light in the visible to infrared range to non-invasively measure the spatial distributions of the optical absorption coefficient (μ_a) and scattering coefficient (μ_s). Though it cannot offer anatomical images with as good spatial resolution as MRI, it can provide better

* Corresponding authors' emails: James M. Masciotti: (jmm2014@columbia.edu), Andreas H. Hielscher: (ahh2004@columbia.edu)

temporal resolution, which ranges from 1Hz to 35 Hz. With diffuse optical tomography, tissue is illuminated and the amount of light that exits the tissue at different positions is measured in order to determine how much the light has been attenuated by the optical absorption and scattering inside tissue. Mathematical models of how light propagates in tissue are used to reconstruct the tissue's spatial distributions of absorption and scattering from the collected measurements [8]. The sensitivity of absorption and scattering coefficients to any given chromophore varies with wavelength. Therefore, by taking measurements at multiple wavelengths, one can generate maps of spatially varying chromophore concentrations, such as oxyhemoglobin (HbO₂), deoxyhemoglobin (Hb). Combined with the fast data acquisition capability of DOT, a variety of hemodynamic effects can be studied. A common problem encountered in DOT is that the image reconstruction is ill-posed and ill-determined. Therefore, different distributions of optical properties inside the medium can lead to the same optical signals on the surface of the medium. One method of reducing the ill-posedness, is to acquire DOT data in either the time domain or frequency domain instead of the steady-state-domain. We therefore consider here a frequency-domain system.

In the following section we present the design of a frequency-domain optical tomography instrument with an MRI interface that allows for the simultaneous diffuse optical tomography and magnetic resonance imaging of small animals. By combining DOT and MRI we can capture anatomical and physiological information with high spatial and temporal resolution [9]. By overlaying the time varying physiological optical images on the high spatial resolution MRI images, one can observe physiological dynamics and know exactly where they occur anatomically. The anatomical information provided by MRI can also be used as a priori information for the reconstruction of the optical images and thereby improve their spatial resolution [10].

2. FREQUENCY DOMAIN OPTICAL TOMOGRAPHY INSTRUMENT

2.1 Frequency Domain Optical Tomography

In diffuse optical tomography, image reconstruction is the process by which a quantitative map of optical properties is calculated. Typically this is done by taking a model of how light travels in tissue, and adjusting the optical properties of the tissue in the model in order to minimize the error between the measured data in the experiment and the predicted measurement values that the model generates [8]. This usually involves using the "forward" model many times in order to generate predicted measurement values for different sets of optical properties. The propagation of light in tissue is commonly modeled by the equation of radiation transport [11-13]. In the frequency domain, light propagates as photon density waves and the equation of radiation transport is written as follows:

$$\frac{j\omega}{v}\psi(\vec{r}, \theta, \omega) + \theta \cdot \nabla \psi(\vec{r}, \theta, \omega) + \mu_a(\vec{r})\psi(\vec{r}, \theta, \omega) + \mu_s(\vec{r}) \left(\psi(\vec{r}, \theta, \omega) - \int_{4\pi} p(\theta \cdot \theta', g)\psi(\vec{r}, \theta', \omega) d\theta' \right) - S(\vec{r}, \theta, \omega) = 0. \quad (1)$$

In this equation ψ is the radiance, r is vector representing the spatial position $r=(x,y,z)$, θ is the angular direction of the radiance, ω is the radial frequency of the photon density wave and v is the velocity of light in tissue which is typically 2.2×10^{10} cm/sec. The absorption and scattering coefficients which are typically in units of cm^{-1} are represented by μ_a and μ_s respectively. The scattering phase function, which is typically modeled by the Henyey-Greenstein function, is represented by p , the anisotropy factor is g , and S is the source. In cases where the scattering coefficient is large and the absorption coefficient is small the frequency domain equation of radiation transport can be approximated by the diffusion equation:

$$\frac{j\omega}{v}U(\vec{r}, \omega) + \mu_a(\vec{r}) - \nabla D(\vec{r}) \nabla U(\vec{r}, \omega) - S_0(\vec{r}, \omega) = 0 \quad (2)$$

U is the fluence which is the summation of the radiance over all directions, S_0 is the source and D is the diffusion coefficient given by:

$$D = \frac{1}{3(\mu_s(1-g) + \mu_a)} \quad (3)$$

Solutions to equation (2) are strongly attenuate waves, commonly referred to as photon-density waves, whose amplitude, speed, and wavelength are dependent on the optical properties μ_a and μ_s . The effective cross section, which can be obtained from the diffusion coefficient, is complex and is given by:

$$\mu_{eff} = \sqrt{\frac{\mu_a + \frac{j\omega}{v}}{D}} \quad (4)$$

The magnitude of the effective cross section shows how much the photon density wave is attenuated by the tissue's optical properties is given by:

$$|\mu_{eff}| = \sqrt{\frac{\mu_a + \sqrt{\mu_a^2 + \frac{\omega^2}{v^2}}}{2D}} \quad (5)$$

As is evident from (5), increasing μ_a , μ_s , or ω will result in more highly attenuated photon density waves. This means the detected signals will be smaller and likewise so will the signal to noise ratio.

2.2 Choice of modulation frequency

One of the reasons that the optical tomography problem is difficult is because the problem is underdetermined. The number of unknown quantities one reconstructs, the values of the absorption and scattering coefficients at different position, are far more than the number of known quantities, the measured detector values, one has to work with. Usually one reduces the ill-determinedness of the problem by taking more acquiring more information. That information only helps to the extent by which it is orthogonal to already acquired information. An example of acquiring more information that is not very orthogonal is using many detectors at essentially the same location. By analyzing (1), one can see that the radial frequency and the absorption coefficient operate on the radiance as a simple multiplication, while the scattering coefficient also multiples with the integral term. It is therefore evident that if the frequency is large enough, $\omega \gg \mu_a$, it will dominate the absorption term and the equation will essentially become independent of absorption. If measurements are taken at low frequencies such as DC, and large frequencies, crosstalk between absorption and scattering can be significantly reduced. Generally, in order to get sufficient reduction in crosstalk, the high modulation frequency needs to be as fairly large, otherwise the high frequency information that is acquired is not sufficient orthogonal to the low frequency information. If we desire to have the contribution of the absorption coefficient to (1), reduced by half, then the following must hold:

$$\omega > \sqrt{3}v\mu_a \quad (6)$$

This means that for a μ_a of 0.1 cm^{-1} , the radial frequency should be at least as large as $3.8 \times 10^9 \text{ rad/sec}$, which is equivalent to say that the frequency f should be at least as large as 607 MHz. Large frequencies, however, will result in an effective cross section which is larger in magnitude and therefore also will also result in smaller signals, as evident in (5). However in small geometries, such as those encountered in small animals, the signal attenuation by the effective cross section will not be as great as it is in larger geometries. Therefore it is beneficial and feasible to use high frequencies for small animal diffuse optical tomography. Since there is a trade off between crosstalk reduction and signal to noise, an optimal frequency can be found for a given set of optical properties. Finding the optimal frequency has been investigated in [14], and it was found that frequencies up to 800 MHz may be ideal. Our frequency domain optical tomography instrument is capable of using modulation frequencies up to 1 GHz.

2.3 Frequency domain instrument description

Figure 1 shows a diagram of the frequency domain instrument setup in our laboratory. The system employs two laser diodes at 2 different wavelengths $\lambda_1 = 757 \text{ nm}$ and $\lambda_2 = 828 \text{ nm}$. The 2 laser diodes have 3 dB bandwidths of 800 MHz and 700 MHz respectively and 10 dB bandwidths of 1.3GHz. They both are driven by modulated laser drivers and have peltier cooling. The laser diodes are pigtailed into single mode optical fiber. Those 2 fibers are then input to a 2x32 fiber optic switch (that has low coupling losses and fast switching times (4 ms). The fiber optic switch uses standard $62.5 \mu\text{m}$ graded-index multimode fibers which provide good coupling efficiency from the single mode fibers and high bandwidth. Both source and detector fibers are graded-index multimode fibers and interface with the DOT-MRI imaging head which will be described in more detail in section 3. On the instrument side, detector fibers that deliver light from the imaging head have their tips arranged by drilling holes in a thin slab of aluminum. An intensified CCD

camera system (Picostar HR LaVision, Germany) then focuses on the tips of the optical fibers as was done in [15]. In order to maximize the amount of light focused into the Intensifier tube a “close-up” lens was used (60mm f/2.8D) which has a minimum focusing distance of 22 cm. We also have the option of using a moveable graduated ND filter. This allows us to attenuate detectors in relation to how close to they are to the active source, are thereby increase the dynamic range. It is possible to operate the instrument without detector fibers in order to perform non-contact imaging, but the fibers are necessary when imaging inside an MRI magnet.

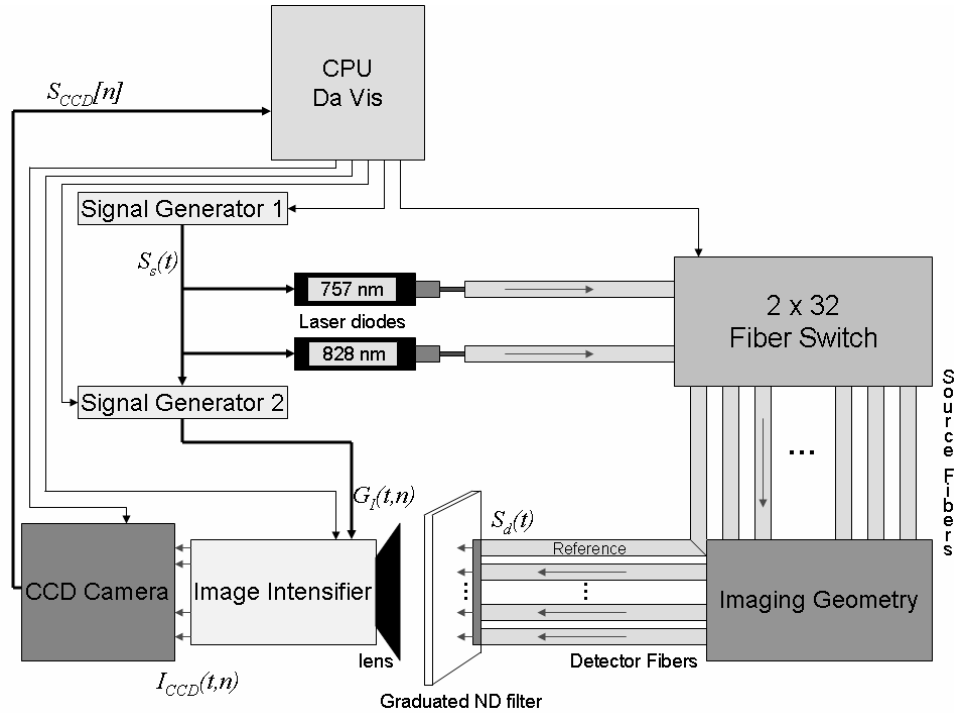


Fig. 1: Diagram of the Frequency Domain Optical Tomography Instrument

The intensifier can be thought of as a photon amplifier and has 3 stages. First light passes through the input window and is incident on the photocathode. The photocathode, when activated by a voltage, converts photons into electrons. These electrons enter and accelerate through a micro channel plate (MCP). The MCP produces a gain in the number of electrons, which depends on the voltage which is applied across the MCP. The electrons exit the MCP and are incident on a phosphor screen where they are converted back to photons. The photons that exit the intensifier are then focused on to the sensor of the CCD camera. The CCD camera has 1376 x 1040 pixels and is triggered by and transfers the acquired images to a PC running DaVis imaging software (LaVision, Germany). Since the detector fibers are only focused onto a small area, the CCD crops the data to a smaller rectangle showing the detector fibers. For each fiber, the pixels showing light from that fiber are averaged to produce one detector value for that fiber. Conventionally a photocathode is gated by a pulse so the intensifier can act like a shutter. In our instrument a sinusoidal voltage is applied across the cathode allowing RF modulation. Similar instruments are described in [16] and [17], but they operate at lower frequencies and have longer acquisition times. The photocathode voltage signal, MCP voltage and other bias voltages are supplied by the High Rate Imager.

2.4 Modulation and demodulation of optical signals

Two signal source generators are used to produce the RF signals that are needed for modulating the laser diodes and the photocathode of the image intensifier. The parameters of the generated signals (amplitude frequency, phase etc.) are computer controlled through the serial port. One signal generator is master and its RF signal is input to the both of the modulated laser drivers. The frequency of the slave signal generator is set to that of the master signal generator. The phase difference between the resulting 2 signals is controlled, which as we will show is necessary to demodulate the optical signal.

The current driving laser diodes can be electronically modulated in order to produce modulated optical source. Since photon density can only be positive, sinusoidal modulation of the optical source signal must take the form of a raised sinusoid.

$$S_s(t) = A_s(1 + m_s) \cos(\omega t + \phi_s) \quad (7)$$

The raised sinusoid is always positive and thus, m_s is less than 1. As the photon density waves travel in tissue, the optical properties will have a system response $H_t(\omega)$, which will consist of a frequency dependant attenuation and phase shift. The measured detector signal will thus take the form of:

$$S_d(t) = A_s(H_t(0) + |H_t(\omega)| m_s \cos(\omega t + \phi_s + \phi_t)) \quad (8)$$

CCD cameras are powerful detectors because the images they acquire can be considered sets of millions of independent measurements (pixels) which can be used to simultaneously measure the amount of light that is incident at many different positions. But because they essentially integrate the detected light over their exposure time, for example 20 ms to 8 s in our system, they are unable to measure fast varying signals. Usually a photodiode is used to measure this modulated optical signal. The signal is then demodulated, most commonly by using lock-in detection, which consists of multiplying the measured signal by sinusoids of the same frequency, in order to measure the amplitude and phase [18]. Digital lock-in detection tends to have high signal to noise ratios [19]. Instead, we modulate the gain of an image intensifier in order to partially demodulate the signal in the optical domain. The gain of the intensifier G_I , is also a raised sinusoid which prevents standard demodulation techniques, but we take several, n , measurements and while modulating the gain, incremental phase shifts, $\Delta\phi_I$, are added.

$$G_I(t, n) = A_I(1 + m_I \cos(\omega t + n\Delta\phi_I)) \quad (9)$$

The light intensity that is incident on the CCD, I_{CCD} , is a product of the detector signal and the gain signal, and contains 2 DC terms and many high frequency terms (HFT)

$$I_{CCD}(t, n) = G_I(t, n) \times S_d(t) = A_I A_s H_t(0) + A_I A_s \frac{m_I m_s}{2} |H_t(\omega)| \cos(\phi_s + \phi_t - n\Delta\phi_I) + HFT. \quad (10)$$

The light incident on the CCD is integrated over the exposure time. Since the exposure time is much longer than the modulation period, this leaves only the DC terms

$$S_{CCD}[n] = \int_{t_e} I_{CCD}(t, n) dt = A_I A_s t_e H_t(0) + A_I A_s t_e \frac{m_I m_s}{2} |H_t(\omega)| \cos[\phi_s + \phi_t - n\Delta\phi_I]. \quad (11)$$

Because the product of the S_d and G_I is sampled at discrete phase offsets this technique can be thought of as a phase sampling heterodyne technique that produces a discrete signal with N_s , samples. It has however previously been referred to as homodyne detection [16,17].

The quantities of interest of the signal in (11) are the DC term, the amplitude of the sinusoid, and the phase of the sinusoid. We use a digital lock-in filtering technique that has been shown to be ideal for determining the DC, amplitude and phase for this type of signal [20]. The main requisite for this technique is that (11) be sample over an integer number of periods, N_p , and that the nyquist criterion is held. For fast measurements, during which we set the exposure time to 20 ms, it is best to set N_p to 1 period. The nyquist criterion will tell us that more than 2 phase samples per period will be needed. Since taking 4 samples will provide far better filtering than 3, we set N_s to 4 and thus make $\Delta\phi_I$ equal to $\pi/2$ and the total measurement time for a source equal to 80 ms. The DC term can be found by complete overlap filtering the signal with the following N_s point filter:

$$h_{DC}[n] = \frac{1}{N_s}, \quad (12)$$

$$A_I A_s t_e H_t(0) = \sum_{n=1}^{N_s} h_{DC}[n] \times S_{CCD}[n], \quad (13)$$

which is equivalent taking the mean. The amplitude and phase can be found by complete overlap filtering the signal with the following complex valued filter:

$$h_{AC}[n] = \frac{2}{N_s} \cos\left[\frac{N_p}{N_s} 2\pi\right] + \frac{2j}{N_s} \sin\left[\frac{N_p}{N_s} 2\pi\right], \quad (14)$$

The amplitude will and phase will just be the amplitude and phase of the complex valued filter output as discussed in [20].

$$A_I A_{St_e} \frac{m_1 m_2}{2} |H_t(\omega)| = \left| \sum_{n=1}^{N_s} h_{AC}[n] \times S_{CCD}[n] \right| \quad (15)$$

$$\phi_s + \phi_t = \arg\left(\sum_{n=1}^{N_s} h_{AC}[n] \times S_{CCD}[n] \right), \quad (16)$$

Eventually, $H_t(0)$, $|H_t(\omega)|$, and ϕ_t are found after calibrating for the other terms with a reference. Nonlinearities in the signals in (8) and (9) can introduce errors in measurements. When harmonic distortion exists for both signals at the same harmonic, nothing can be done. However when the harmonic distortion of the 2 signals do not occur at the same frequency, one can filter out these distortions by taking enough samples per period. By taking 4 samples per period, we have immunity to the second harmonic, which is usually the largest harmonic.

2.5 Experimental Data

To test the frequency domain system and the demodulation technique a simple phantom experiment was setup. The instrument was used in non-contact imaging mode without detector fiber or the optical switch. A single pigtailed laser diode modulated at 500 MHz was used to illuminate the side of a square plastic bottle which was filled with 1% Intralipid. The source was placed close to the front face of the bottle and the intensified CCD camera focused on the surface of the front face of the bottle. The integration time, t_e , was set to 20 ms, and 32 phase step images were acquired. The amplitude and phase were then calculated as described above, and are shown in fig 2.

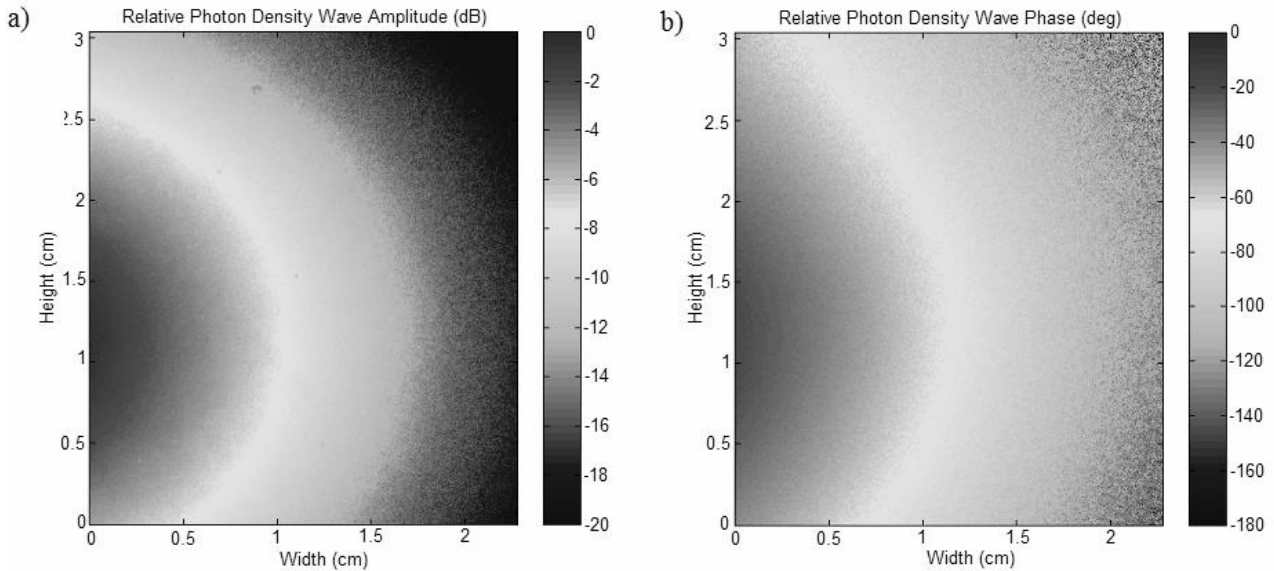


Fig. 2: Calculated amplitude a) and phase b) for test setup with 1% Intralipid and 500 MHz modulation frequency.

3. SMALL ANIMAL OPTICAL TOMOGRAPHY – MRI INTERFACE

3.1 Small animal MRI system

Our small animal MRI system consists of a 9.4 T vertical bore magnet and a Bruker Avance 400 spectrometer. It is equipped with exchangeable gradient coils. For mouse imaging the micro2.5 gradient set is used which consists of a 2.5 guass/cm/A gradient coil with an inner diameter of 4 cm, and RF birdcage coils tuned to 400 MHz with an inner diameters ranging from 3 to 3.3 cm. For larger rodents such as rats, the mini 0.75 gradient set is used, which utilizes a 0.75 guass/cm/A gradient coil. It has a larger inner diameter of 5.7 cm which allows for RF coils with inner diameters up to 3.8 cm. A similar combined instrument is described in [21], however, that instrument uses a 4T MRI system which is unable to image mice at such high resolutions. It also has fewer source detector pairs and is limited to a modulation frequency of 300 MHz.

3.2 Optical Imaging Head

The confines of these small inner diameter MRI coils do not leave much room for an optical imaging head. It prohibits the use of large optical fibers and most fiber jacketing. It also makes it difficult to couple light between the optical fibers, which must travel from the frequency domain instrumentation, up into the imaging space of the vertical bore magnet and then back for a total distance of 25 m. Unlike what is done in [21], there is not enough room for a sophisticated method that ensures direct fiber contact with the animal. Therefore we have chosen to use a static cylindrical geometry which is filled with matching fluid and has fibers connected to the surface, similar to the one in [9]. Light couples into a medium best when it is incident at a normal angle to a surface and there are two main methods to accomplish this. Small right angle prisms could be placed on the tips of the fibers in order to reflect light between the fiber tip and the cylinder's surface [22] or the fiber could be bent into contact with surface of the geometry. While the first option can be more compact, we find that they can be difficult to affix and wind up being very expensive when a large number of fibers are used. We choose to use fibers with small bending radii to couple the light into and out of the medium. Large core fibers are usually used as detector fibers because they are able to collect more light. Our optical signals travel at high modulation frequencies over long distances which causes multimode distortion in step-index fibers. This fact and our need for good coupling of light require us to use graded index multimode fibers. Large core graded index fibers are rare and tend to have large bend radii. We chose source fibers with 100- μm core diameter and 250- μm coating diameter and a bandwidth of 100 MHz/km and detector fibers with 200 μm core diameter and 450 μm coating diameter and bandwidth of 100 MHz/km. Then at the tip of each fiber we attach a short segment, 5 cm, of 250 μm step index plastic fiber which has a small bending radius of 2 mm. This small segment of step index fiber is bent at a quarter turn in order to couple light onto the surface of the geometry at a normal angle.

3.3 Coregistration with MRI

Simultaneously acquiring MRI images along with Optical Tomography data allows MRI to aid Optical Tomography in many ways. Besides simply comparing images from the 2 modalities, MRI images can be used to generate a 3D geometry or mesh, and can be used as apriori information. Before this can be done, it is necessary to be able to coregister the 2 images so that they can be related to each other. When doing this, it is necessary to know the positions of the source and detector positions so that one can create the correct forward model for optical tomography reconstructions. Coregistration is normally accomplished by including fiducial markers for one or more of the modalities. Since MRI has better spatial resolution than DOT, it is generally better to use fiducial markers that appear in MRI images. A good fiducial marker will come out bright in an image and be located in its correct location in the image. Since the brightness will be proportional to the partial volume of the marker in the MRI voxel, most MRI fiducial markers designed for humans have sizes on the order of centimeters. This presents a challenge for our compact small animal imaging system. Our solution consists of using small catheters, which are 0.58 mm inner diameter and 1 mm in outer diameter, and are filled with the liquid that is used in a commercially available human MRI fiducial marker (Radiance®). Radiance® appears bright in just about all MRI image regardless of contrast mechanism. The catheters are cut, sealed, and strategically placed. An example image of the catheters placed around a water phantom is shown in fig. 3. The catheters can be placed adjacent to each fiber or used to define a plane in space on which a group of fibers are located.

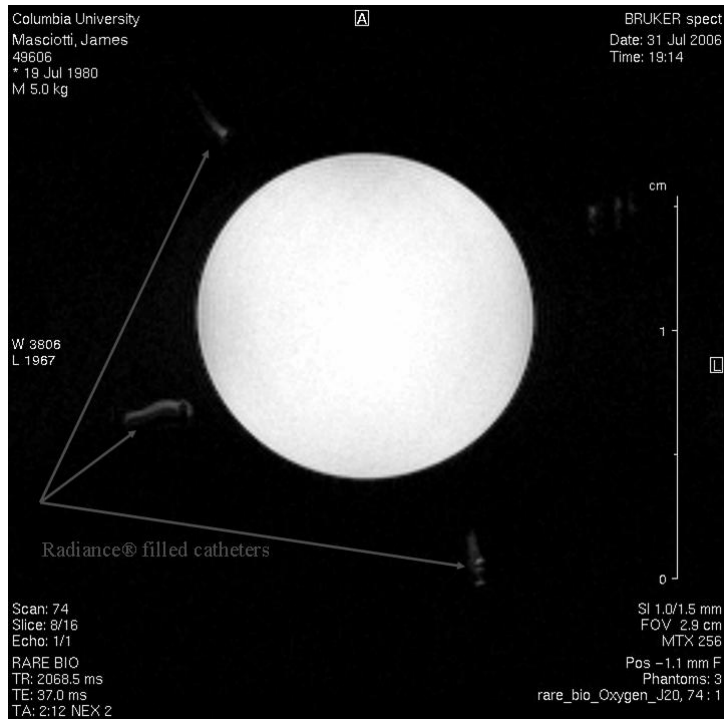


Fig. 3: MRI image of Radiance® filled catheters positioned around a water phantom.

4. CONCLUSION

In this work we have described design considerations for a frequency-domain instrument that can be used to obtain simultaneous optical tomographic and magnetic resonance images of small animals. We found that it is desirable and feasible to use source-modulation frequencies above 400 MHz to image small animals and, unlike existing systems, our CCD camera based instrument is capable of source-modulation frequencies up to 1 GHz. We have described how amplitude and phase information can be obtained using a digital lock-in filter, and presented design details of an optical imaging head that can be placed inside a 9.4T MR micro-imager. Future work will consist of completing tests on the instrument and using it for in vivo imaging of small animals.

ACKNOWLEDGEMENTS

This work was supported in part by the National Institute of Biomedical Imaging and Bioengineering (NIBIB grant 5R01-EB001900), which is part of the National Institutes of Health (NIH).

REFERENCES

1. S.R. Cherry, "In vivo molecular imaging and genomic imaging: new challenges for imaging physics," *Phys. Med. Biol.* **49**, R13 (2004).
2. M. G. Pomper, "Can small animal imaging accelerate drug development?" *Journal Cellular Biochemistry Suppl.* **39**, pp. 211-220. (2002).
3. H. Benveniste, S. Blackband, "MR microscopy and high resolution small animal MRI: applications in neuroscience research," *Prog. Neurobiol.* **67** pp. 393-420 (2002).
4. E. X. Wu, K. K. Wong, M. Andrassy, H. Tang, "High-resolution in vivo CBV mapping with MRI in wild-type mice," *Magnetic Resonance in Medicine* **49**(4), pp. 765-770 (2003).

5. A.H. Hielscher, "Optical tomographic imaging of small animals," *Current Opinion in Biotechnology* **16**(1), pp. 79-88 (2005).
6. G. A. Wright, "Magnetic resonance imaging," *IEEE Signal Processing Magazine* **14** pp. 55-66 (1997).
7. A. P. Gibson, J. C. Hebden, S. R. Arridge, "Recent advances in diffuse optical imaging," *Phys. Med. Biol.* **50** pp. R1-R43 (2005).
8. S. R. Arridge, "Optical tomography in medical imaging", *Inverse Problems* **15** pp. R41-R93 (1999).
9. J. Masciotti, F. Provenzano, J. Papa, A. Klose, J. Hur, X. Gu, D. Yamashiro, J. Kandel, A.H. Hielscher, "Monitoring tumor growth and treatment in small animals with magnetic resonance and optical tomographic imaging," in *Multimodal Biomedical Imaging*, F. S. Azar, D. N. Metaxas, eds., Proc. 6081, pp. 608105-1 – 608105-9 (2006).
10. M. Guven, B. Yazici, X. Intes, B. Chance, "Diffuse optical tomography with apriori anatomical information", *Phys. Med. Biol.* **50** pp. 2837-2858 (2005).
11. A. D. Klose, U. Netz, J. Beuthan, A. H. Hielscher, "Optical tomography using the time-independent equation of radiative transfer. Part 1: Forward model," *J. Quantitative Spectroscopy and Radiative Transfer*, **72** pp. 691-713 (2002).
12. A. D. Klose, A. H. Hielscher, "Optical tomography using the time-independent equation of radiative transfer. Part 2: Inverse model," *J. Quantitative Spectroscopy and Radiative Transfer*, **72** pp. 715-732 (2002).
13. K. Ren, G. Bal, A. H. Hielscher, "Frequency-domain optical tomography based on the equation of radiative transfer," *SIAM Journal of Scientific Computing* **28** pp. 1463-1489 (2006).
14. X. Gu, K. Ren, A. H. Hielscher, "Frequency-domain sensitivity analysis for small imaging domains using the equation of radiative transfer." (To be published in *Applied Optics*).
15. J. Selb, D. K. Joseph, D. A. Boas, "Time-gated optical system for depth-resolved functional brain imaging", *J. Biomedical Optics*, **11** pp. 044008-1 – 044008-13 (2006).
16. J. S. Reynolds, T. L. Troy, E. M. Sevick-Muraca, "Multipixel Techniques for Frequency-Domain Photon Migration Imaging," *Biotechnol. Prog.* **13** pp. 669-680 (1997).
17. A. B. Thompson, E. M. Sevick-Muraca, "Near-infrared fluorescence contrast-enhanced imaging with intensified charge-coupled device homodyne detection: measurement precision and accuracy," *Journal of Biomedical Optics* **8** pp. 111-120 (2003).
18. C. H. Schmitz, M. Locker, J. M. Lasker, A. H. Hielscher, R. L. Barbour, "Instrumentation for fast functional optical tomography," *Rev. Sci. Instrum.* **73** pp. 429-439 (2002).
19. L. A. Barragan, J. I. Artigas, R. Alonso, F. Villuendas, "A modular, low-cost, digital signal processor-based lock-in card for measuring optical attenuation," *Rev. Sci. Instrum.* **72** pp. 247-251 (2001).
20. J. M. Masciotti, J. M. Lasker, A. H. Hielscher, "Digital lock-in algorithm for biomedical spectroscopy and imaging instruments with multiple modulated sources", *Engineering in Medicine and Biology Society, 2006. EMBS '06. 28th Annual International Conference of the IEEE* pp. 3198-3201 (2006).
21. G. Gulsen, O. Birgul, M. Burcin, R. Shafiiha, O. Nalcioglu, "Combined diffuse optical tomography (DOT) and MRI system for cancer imaging in small animals," *Technology in Cancer Research and Treatment* **5** pp. 351-363 (2006).
22. U. Utzinger, R. R. Richards-Kortum, "Fiber optic probes for biomedical optical spectroscopy," *Journal of Biomedical Optics* **8** pp. 121-147 (2003).